Electronic Supplementary Material (ESI) for Energy & Environmental Science.

Electronic Supplementary Information for

Intramolecular electronic coupling in porous iron cobalt (oxy)phosphide nanoboxes enhances the electrocatalytic activity for oxygen evolution

Huabin Zhang,[a] Wei Zhou,[b] Juncai Dong,[c] Xuefeng Lu[a] and Xiong Wen (David) Lou[a]*

[a] School of Chemical and Biomedical Engineering, Nanyang Technological University,62 Nanyang Drive, Singapore, 637459, Singapore.

E-mail: xwlou@ntu.edu.sg, davidlou88@gmail.com; Web: http://www.ntu.edu.sg/home/xwlou/

[b] Department of Applied Physics, Tianjin Key Laboratory of Low Dimensional Materials Physics and Preparing Technology, Faculty of Science, Tianjin University, Tianjin 300072, China.

[c] Beijing Synchrotron Radiation Facility (BSRF), Institute of High Energy Physics, Chinese Academy of Sciences, Beijing 100049, China.

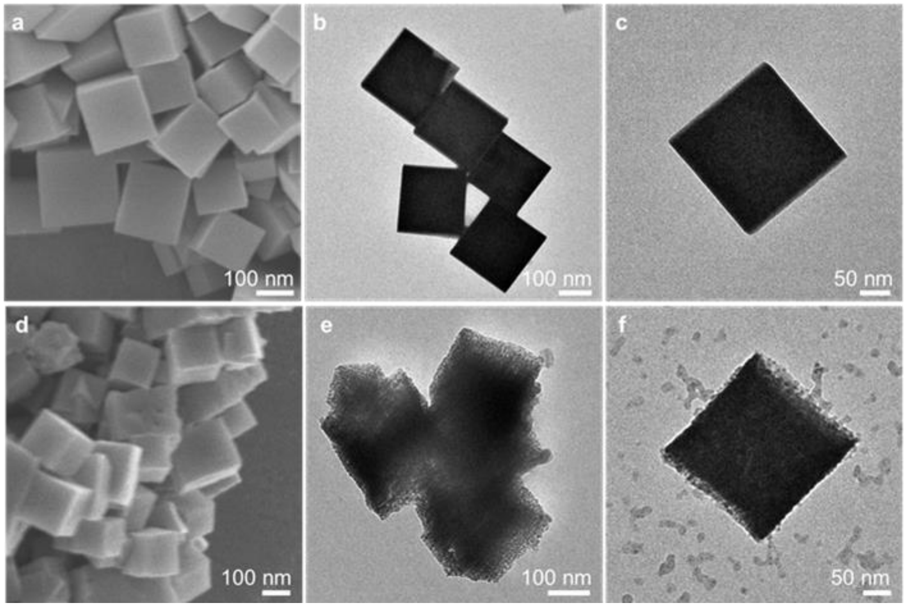

Fig. S1 (a) FESEM image and (b, c) TEM images of Fe-Co PBA nanocubes. (d) FESEM image and (e, f) TEM images of Fe-Co-P nanocubes.

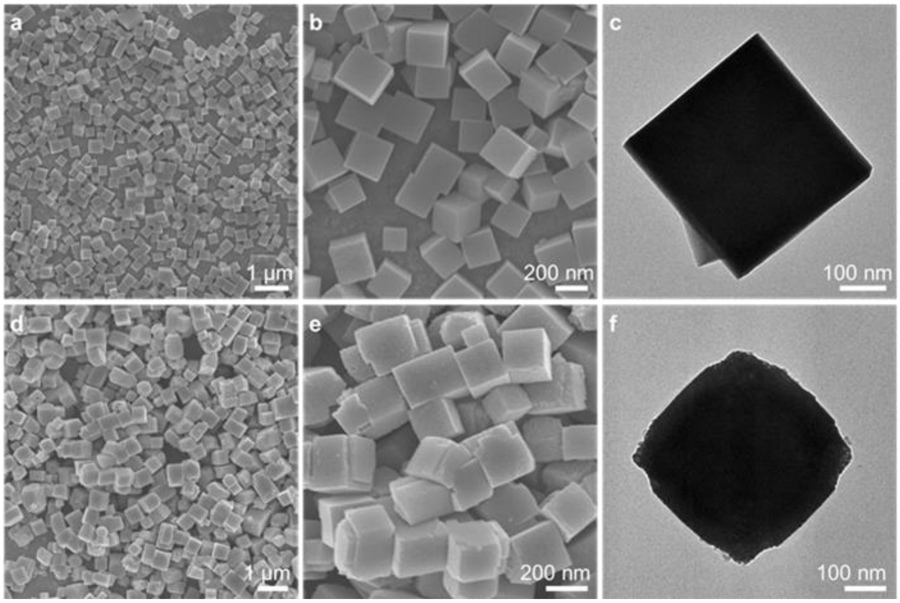

Fig. S2 (a, b) FESEM images and (c) TEM image of Fe-Fe PBA nanocubes. (d, e) FESEM images and (f) TEM image of Fe-P nanocubes.

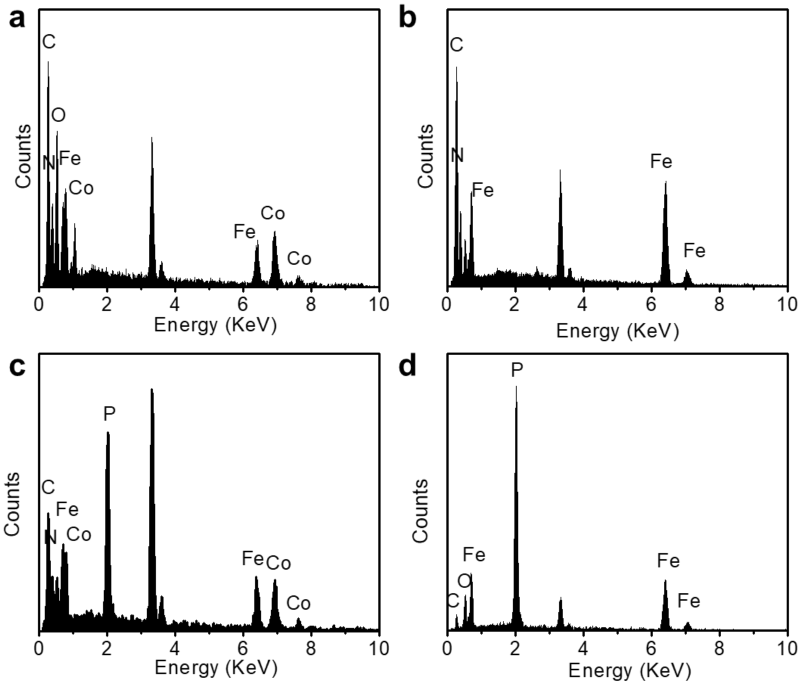

Fig. S3 EDX spectra of (a) Fe-Co PBA, (b) Fe-Fe PBA, (c) Fe-Co-P and (d) Fe-P.

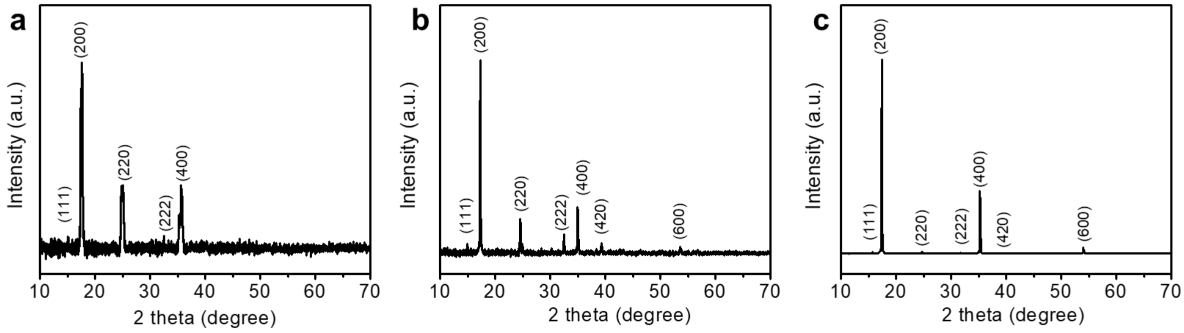

Fig. S4 XRD patterns of (a) Fe-Co PBA nanoboxes, (b) Fe-Co PBA nanocubes and (c) Fe-Fe PBA nanocubes.

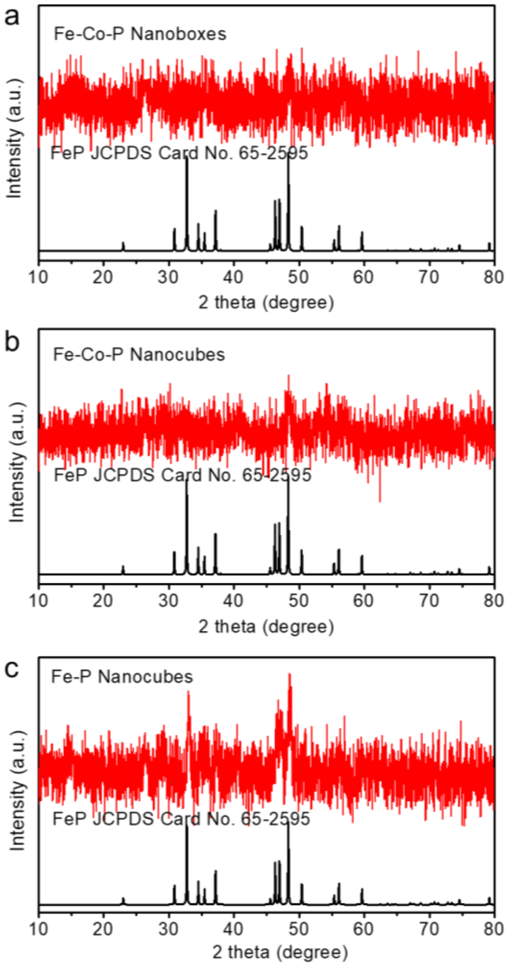

Fig. S5 XRD patterns of (a) Fe-Co-P nanoboxes, (b) Fe-Co-P nanocubes and (c) Fe-P nanocubes.

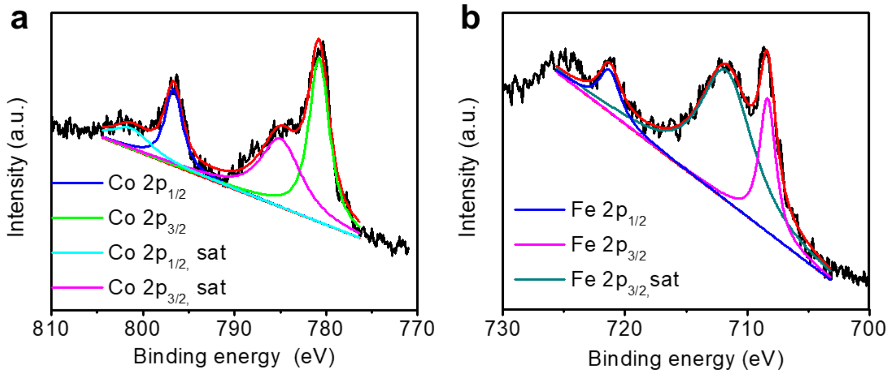

Fig. S6 XPS spectra of (a) Co 2p and (b) Fe 2p of Fe-Co-P.

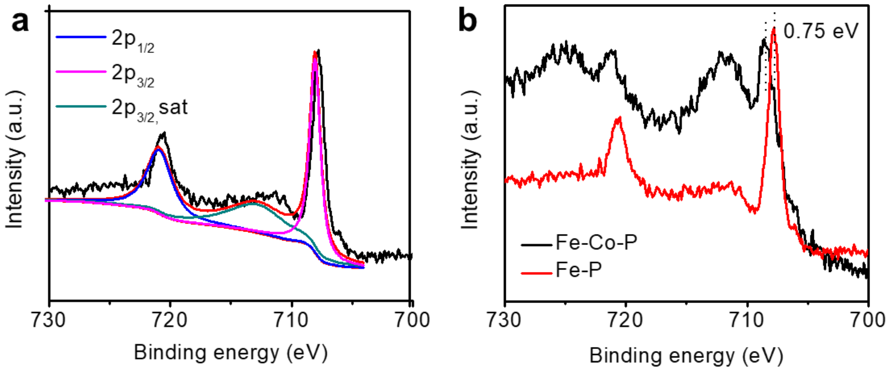

Fig. S7 (a) XPS Fe 2p spectra of Fe-P. (b) Comparison of the Fe 2p spectra between Fe-Co-P and Fe-P. The shift of the Fe 2p spectrum clearly demonstrates the occurring of the electronic coupling between the Fe and Co atoms in Fe-Co-P.

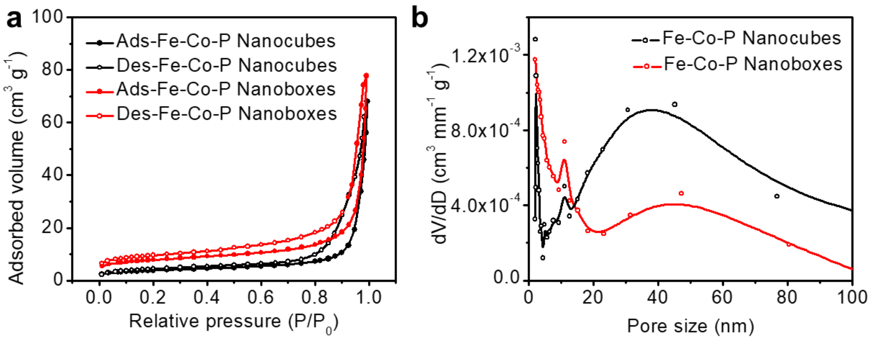

Fig. S8 (a) N_2 adsorption-desorption isotherms for Fe-Co-P nanocubes and Fe-Co-P nanoboxes. (b) Pore size distribution curves for Fe-Co-P nanocubes and Fe-Co-P nanoboxes.

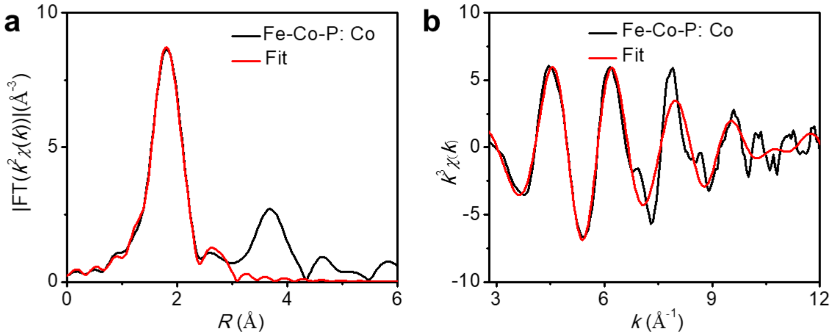

Fig. S9 Experimental and best-fitted EXAFS spectra of Fe-Co-P nanoboxes in (a) *R* space and (b) *K* space. The experimentally measured spectra match well with the calculated spectra for the sample. The best-fit parameters are shown in Table S1.

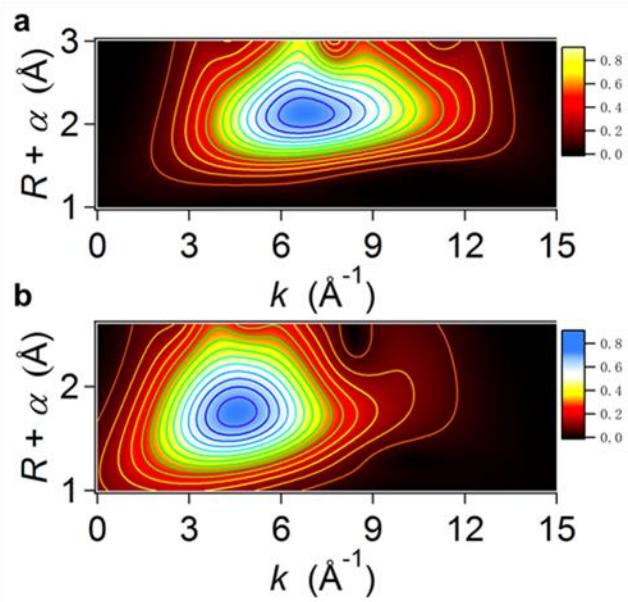

Fig. S10 WT for the k^3-weighted EXAFS signals of (a) Co foil and (b) Fe-P.

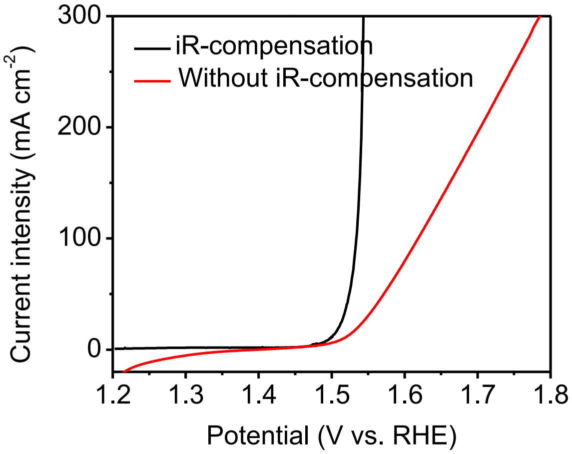

Fig. S11 LSV curves of Fe-Co-P nanoboxes with *iR*-compensation and without *iR*-compensation.

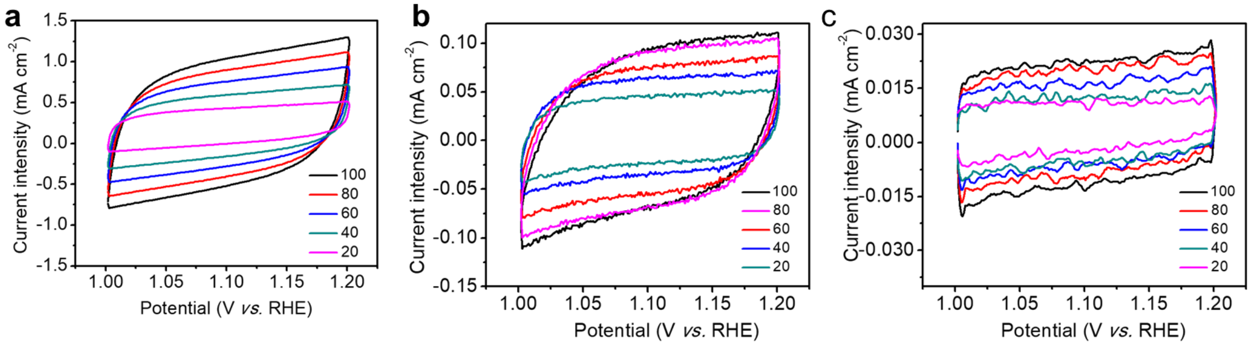

Fig. S12 Cyclic voltammetry curves at different scan rates (mV s^{-1}) for the (a) Fe-Co-P nanoboxes, (b) Fe-Co-P nanocubes and (c) Fe-P nanocubes.

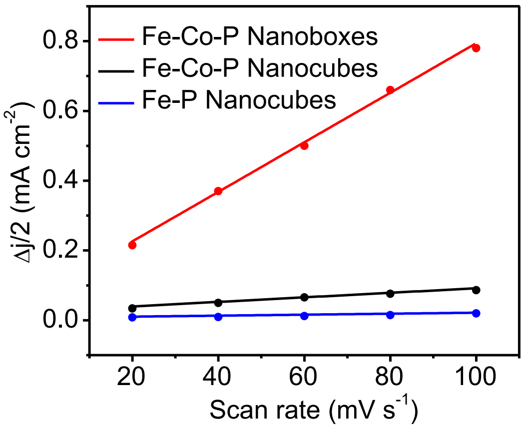

Fig. S13 Capacitive $\Delta j/2 = (j_a - j_c)/2$ as a function of the scan rate for Fe-Co-P nanoboxes, Fe-Co-P nanocubes and Fe-P nanocubes. j_a represents the anodic current density; j_c represents the cathodic current density.

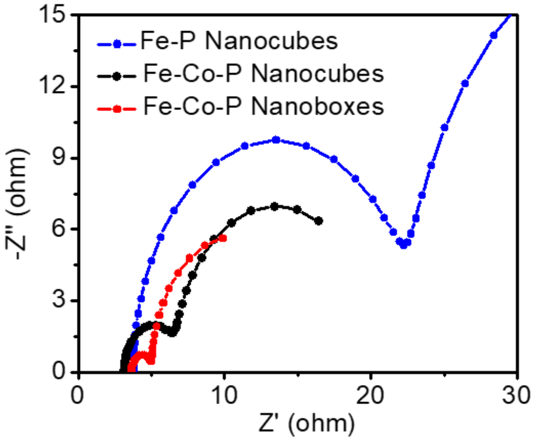

Fig. S14 Nyquist plots of Fe-P nanocubes, Fe-Co-P nanocubes and Fe-Co-P nanoboxes.

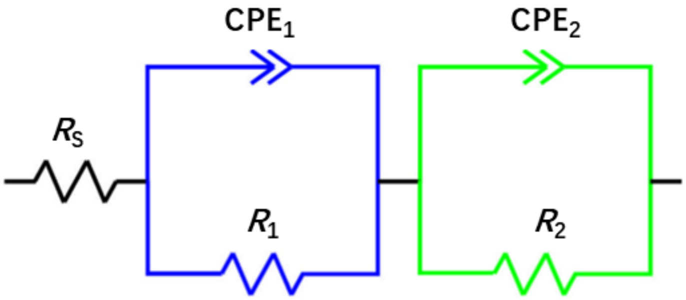

Fig. S15 The two-time constant serial (2TS) model is used for fitting the impedance spectra of Fe-P nanocubes, Fe-Co-P nanocubes and Fe-Co-P nanoboxes. The R_1||CPE1 subcircuit is related to the resistance of the solution filling the pores (R_1, higher frequencies), while the R_2||CPE2 subcircuit refers to charge transfer kinetics (R_2, lower frequencies).

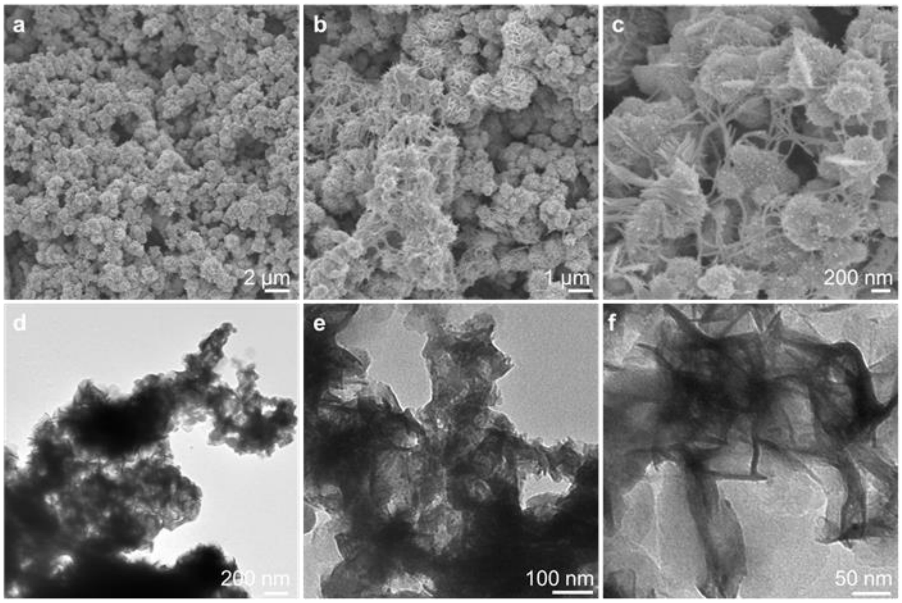

Fig. S16 (a-c) FESEM and (d-f) TEM images of Fe-Co-P nanoboxes after the electrocatalysis.

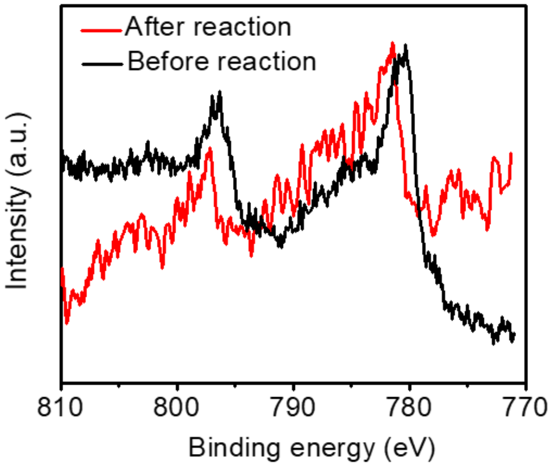

Fig. S17 XPS Co 2p spectra of Fe-Co-P nanoboxes before and after catalysis.

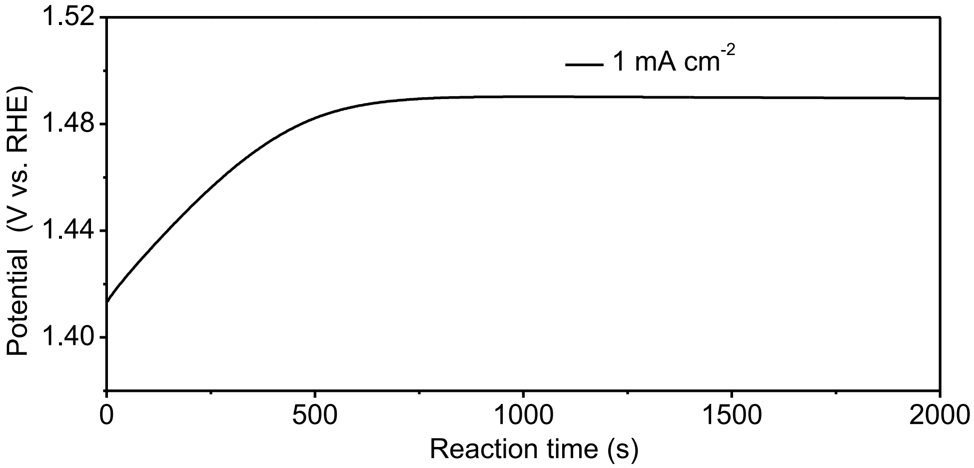

Fig. S18 Chronopotentiometry curve of Fe-Co-P nanoboxes at low current intensity of 1 mA cm^{-2}, monitoring the change of the structure.

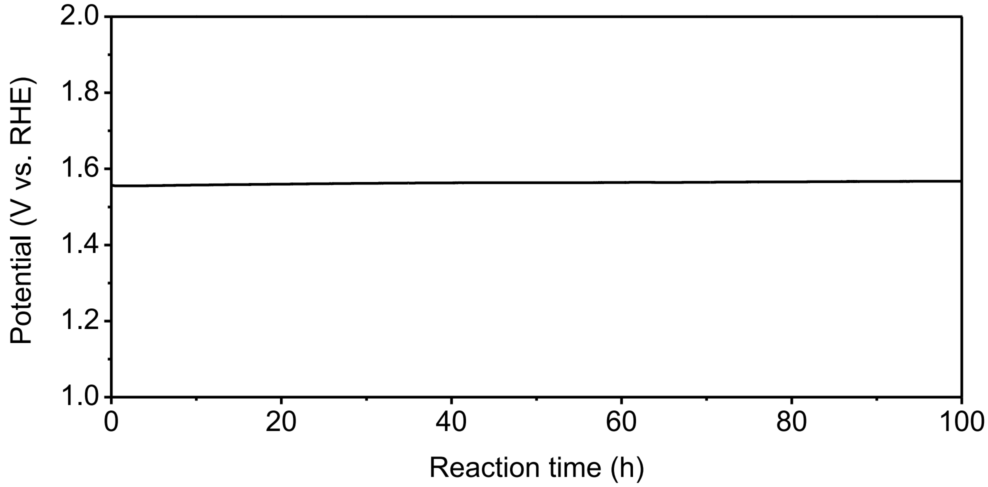

Fig. S19 Chronopotentiometry response at the current density of 30 mA cm^{-2} for Fe-Co-P-O nanoboxes, no *iR*-compensation is applied.

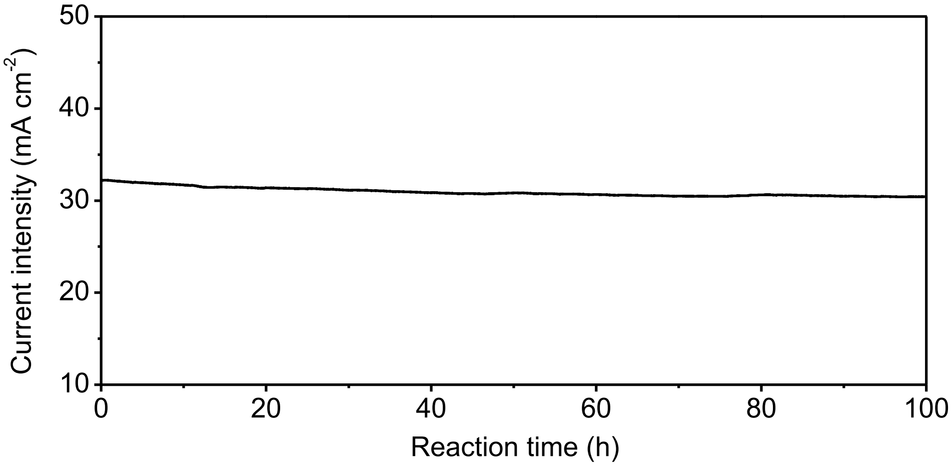

Fig. S20 Time dependence of the current density of Fe-Co-P-O nanoboxes under the fixed potential (1.55 V), no *iR*-compensation is applied.

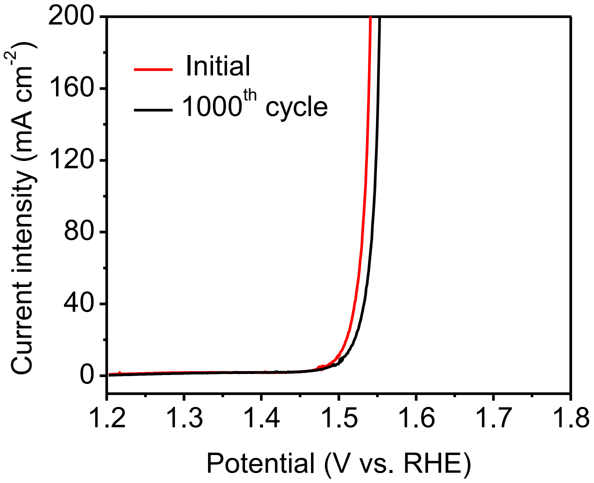

Fig. S21 LSV curves of the Fe-Co-P-O nanoboxes for the initial and the 1000th cycle.

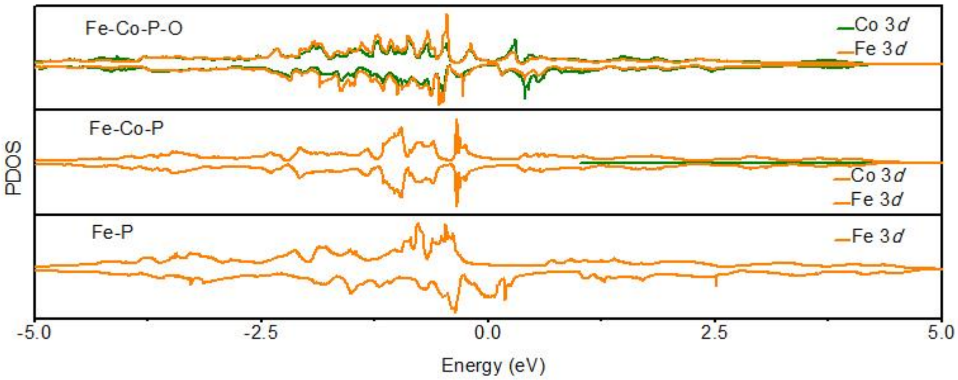

Fig. S22 PDOS for Fe-Co-P-O, Fe-Co-P and Fe-P.

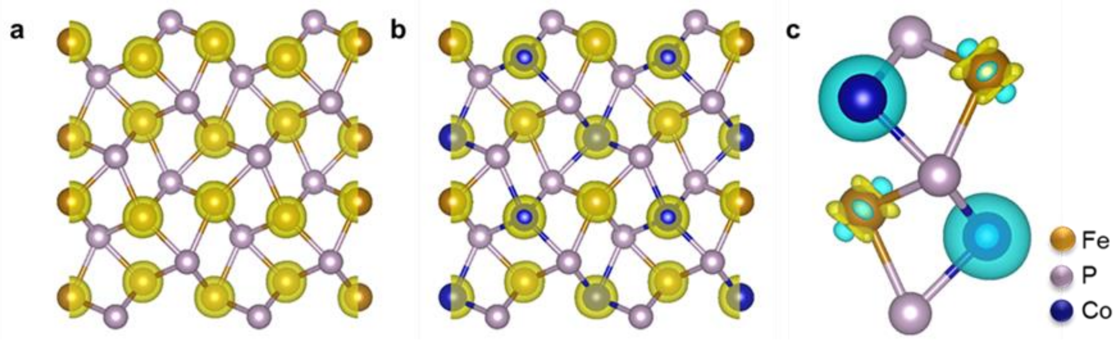

Fig. S23 Calculated distribution of charge densities of (a) Fe-P and (b) Fe-Co-P. (c) Enlarged view of the redistribution for the electron density of Fe-Co-P.

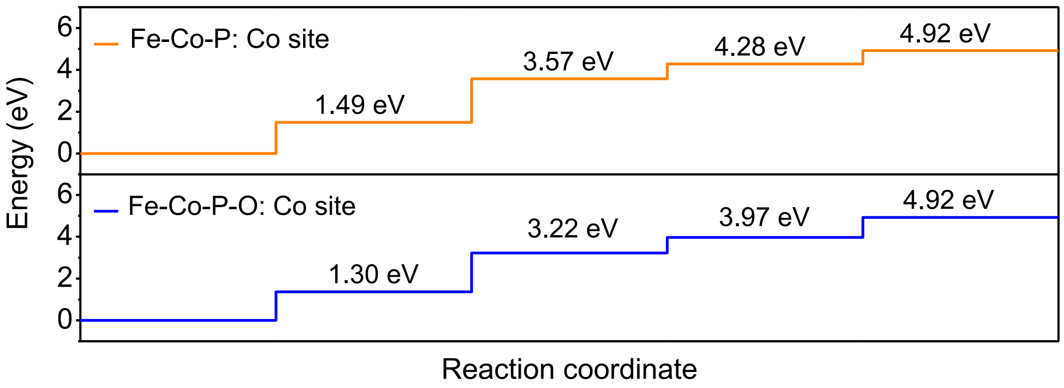

Fig. S24 Free energy diagram for OER over Co sites.

Table S1. *K*-edge EXAFS curve fitting parameters.[a]

Sample	**Shell**	***N***	***R*** (Å)	σ^2 (Å^2)	ΔE_0 (eV)	R_f, %
Fe foil[b]	Fe-Fe	**8**	2.47	0.006	0.7	0.01
	Fe-Fe	**6**	2.85	0.007		
Co foil[b]	Co-Co	12	2.49	0.007	0.7	0.01
Fe-P: Fe[c]	Fe-P	5.5	2.27	0.012	-0.4	0.01
Fe-Co-P: Fe[c]	Fe-P	4.7	2.26	0.013	0.6	0.02
Fe-Co-P: Co[d]	Co-P	4.5	2.24	0.008	-5.5	0.03

[a] *N*, coordination number; *R*, distance between absorber and backscatter atoms; σ^2, Debye–Waller factor to account for both thermal and structural disorders; ΔE_0, inner potential correction; *R*-factor (R_f, %) indicates the goodness of the fitting. Errors are given in brackets. S_0^2 was fixed to be 0.9 both for Fe and Co fitting. Bold numbers indicate fixed coordination number according to the crystal structure.

[b] Fitting range: $3.2 \le k$ (/Å) ≤ 12.5 and $1.4 \le R$ (Å) ≤ 2.7.

[c] Fitting range: $2.0 \le k$ (/Å) ≤ 12.0 and $1.0 \le R$ (Å) ≤ 2.6.

[d] Fitting range: $2.8 \le k$ (/Å) ≤ 12.0 and $1.0 \le R$ (Å) ≤ 2.6.

Table S2. Summary of various metal phosphide-based catalysts for OER.

Catalyst	**η at 10 mA cm^{-2}** (mV)	**Tafel slope** (mV decade^{-1})	**Reference**
MnCoP nanoparticles	330	95	*J. Am. Chem. Soc.* **2016**, *138,* 4006
Co-P film	345	47	*Angew. Chem. Int. Ed.* 2015, 54, 6251
NiCoP@NF	280	87	*Nano Lett.* 2016, 16, 7718
Nanoporous $(Co_{0.52}Fe_{0.48})_2P$	338	30	*Energy Environ. Sci.* 2016, 9, 2257
Ni_2P nanoparticles	290	47	*Energy Environ. Sci.* 2015, 8, 2347
Ni_5P_4	320	40	*Angew. Chem. Int. Ed.* 2015, 54, 12361
Mn-Co oxyphosphide	370	66	*Angew. Chem. Int. Ed.* 2017, 56, 2386
NiCoP/C nanoboxes	330	96	*Angew. Chem. Int. Ed.* 2017, 56, 3897
Fe-Co-P nanoboxes	269	31	This work

Table S3. Impedance parameters obtained by fitting the experimental data in Figure S14.

Electrocatalyst	R_s (Ω cm^2)	R_1 (Ω cm^2)	R_2 (Ω cm^2)
Fe-P nanocubes	3.78	37.57	18.68
Fe-Co-P nanocubes	3.15	3.46	13.85
Fe-Co-P nanoboxes	3.65	1.37	11.39

Table S4. *K*-edge EXAFS curve fitting parameters of Fe-Co-P.[a]

Sample	**Shell**	***N***	***R*** (Å)	$\boldsymbol{\sigma^2}$ (Å^2)	$\boldsymbol{\Delta E_0}$ (eV)	$\boldsymbol{R_f}$, %
Before reaction[b]	Fe−O[c]	1.8	2.01	0.005	3.1	0.1
	Fe−P	4.4	2.31	0.015		
After reaction[d]	Fe−O	4.2	1.98	0.009	2.8	0.1
	Fe−P	2.1	2.30	0.017		

[a] *N*, coordination number; *R*, distance between absorber and backscatter atoms; σ^2, Debye–Waller factor to account for both thermal and structural disorders; ΔE_0, inner potential correction; *R*-factor (R_f, %) indicates the goodness of the fit. Errors are given in brackets. [b] Fitting range: 2.0 ≤ k (/Å) ≤ 11.5 and 1.0 ≤ R (Å) ≤ 2.2. [c] The sample reacted with the alkaline electrolyte before catalysis, resulting in the coordination of O atoms. [d] Fitting range: 2.0 ≤ k (/Å) ≤ 11.5 and 1.0 ≤ R (Å) ≤ 2.2.